

STM/STS Study on $4a \times 4a$ Electronic Charge Order of Superconducting $\text{Bi}_2\text{Sr}_2\text{CaCu}_2\text{O}_{8+\delta}$

Naoki MOMONO, Akihiro HASHIMOTO, Yasuo KOBATAKE, Migaku ODA, and Masayuki IDO

Division of Physics, Graduate School of Science, Hokkaido University, Sapporo 0600810

We performed low-bias STM measurements on underdoped Bi2212 crystals, and confirmed that a two-dimensional (2D) superstructure with a periodicity of four lattice constants ($4a$) is formed within the Cu-O plane at $T < T_c$. This $4a \times 4a$ superstructure, oriented along the Cu-O bonding direction, is nondispersive and more intense in lightly doped samples with a zero temperature pseudogap (ZTPG) than in samples with a d-wave gap. The nondispersive $4a \times 4a$ superstructure was clearly observed within the ZTPG or d-wave gap, while it tended to fade out outside the gaps. The present results provide a useful test for various models proposed for an electronic order hidden in the underdoped region of high- T_c cuprates.

KEYWORDS: STM/STS, pseudogap, electronic charge ordering, superstructure, cuprate

Recently STM/STS studies on the pseudogap state of $\text{Bi}_2\text{Sr}_2\text{CaCu}_2\text{O}_{8+\delta}$ (Bi2212) at $T > T_c$ have revealed a nondispersive two-dimensional (2D) superstructure with a periodicity of about four lattice constants ($\sim 4a \times 4a$ superstructure) in the map of energy-resolved differential tunneling conductance dI/dV , proportional to the local density of states (LDOS).¹⁾ The nondispersive $4a \times 4a$ structure, electronic in origin, was also reported in the LDOS maps taken on the zero temperature pseudogap (ZTPG) regions of lightly doped $\text{Ca}_{2-x}\text{Na}_x\text{CuO}_2\text{Cl}_2$ (Na-CCOC) and Bi2212 samples.^{2,3)} A similar spatial structure was first observed around the vortex cores of Bi2212 exhibiting a pseudogap-like V-shaped spectrum with no coherence peak.⁴⁾ Such 2D spatial structures have attracted much attention because they can be a possible electronic order hidden in the pseudogap state.

From the LDOS maps taken for the superconducting (SC) state of Bi2212, Hoffman et al. and McElroy et al. reported a strongly dispersive 2D superstructure.^{5,6)} This superstructure has been successfully explained in terms of a quasiparticle scattering interference. Furthermore, Howald et al. found a nondispersive $\sim 4a \times 4a$ superstructure with anisotropy in addition to the weakly dispersive one, and claimed that the nondispersive $\sim 4a \times 4a$ superstructure will be due to the so-called stripe order and coexist with superconductivity.⁷⁻¹⁰⁾ However, the nondispersive $\sim 4a \times 4a$ superstructure was not confirmed in later LDOS measurements on Bi2212 at $T < T_c$.^{1,5)} This inconsistency mainly originates from the difficulty in distinguishing the nondispersive $\sim 4a \times 4a$ superstructure from the weakly dispersive $\sim 4a \times 4a$ one resulting from quasiparticle scattering interference. Since the dispersive features in the LDOS are reduced by integrating the LDOS over a wide range of energy, it is desirable to investigate the nondispersive features of the LDOS by using a conventional STM technique which actually maps the LDOS integrated between E_F and $E_F + eV_s$, where V_s is the sample bias voltage. To clarify whether the nondispersive $4a \times 4a$ electronic superstructure persists in the SC state ($T < T_c$) will promote our understanding of the physics in the underdoped region

In the present study, we performed low-bias STM measurements on underdoped Bi2212 samples, and succeeded in observing an energy-independent $4a \times 4a$ electronic superstructure with a substructure having a periodicity of $4a/3$ in the low-bias STM images, which is essentially the same as the electronic checkerboard order reported by Howald et al. and Hanaguri et al. in LDOS maps of lightly-doped Bi2212 and Na-CCOC.^{2,7)} The present $4a \times 4a$ superstructure is accompanied by a d-wave-like gap or ZTPG, and is discussed in terms of a wide variety of unusual electronic orders proposed for the underdoped region of high- T_c cuprates.

The single crystal of Bi2212 in the present study was grown by the traveling solvent floating zone method. We estimated doping level p of the sample from the SC critical temperature T_c determined from the superconducting diamagnetism and the characteristic temperature T_{max} of the normal-state magnetic susceptibility; T_c and T_{max} follow empirical functions of p respectively.^{11,12)} We performed STM/STS experiments at $T \sim 9$ K on two samples A and B cut from the same single crystal with $T_c \sim 72$ K ($p \sim 0.11$). In the present STM/STS experiments, the sample was cleaved in an ultra-high vacuum at $T \sim 9$ K just before the approach of the STM tip to the cleaved surface in situ. As is well known, Bi2212 crystals are usually cleaved between neighboring Bi-O layers. The excess oxygen atoms within Bi-O layers, which provide holes into Cu-O planes nearby, will be lost to a high degree during the process of cleaving. However, if the cleaving is carried out at very low temperatures, the reduction of excess oxygen atoms, thus hole carriers, will be suppressed to some extent. After the approach of the STM tip to the cleaved surface, we obtained STM images of 512×512 pixels in the constant height mode under various constant sample biases, V_s 's. The differential conductance dI/dV was measured by using a standard lock-in technique with ac bias modulation of 3 mV and a frequency of 4 kHz.

Shown in Fig. 1(a) is a typical STM image measured at $T \sim 9$ K on sample A under a low-bias voltage ($V_s = 30$ mV), which lies within the pairing gap as will be men-

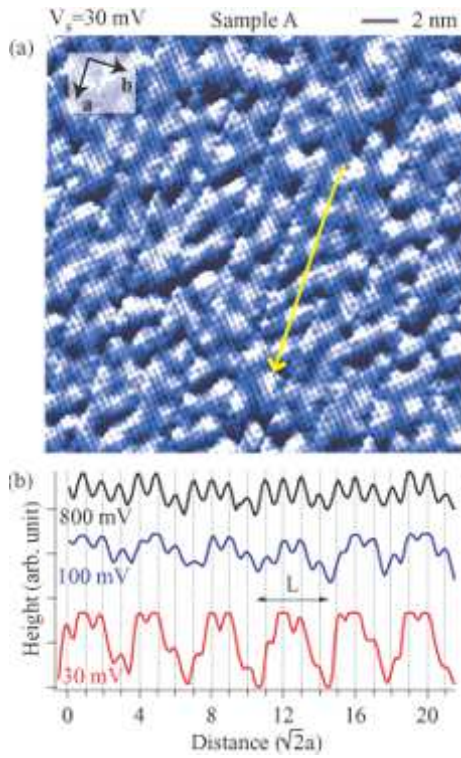


Fig. 1. (a) STM image of sample A at $T \sim 9$ K, showing a $4a \times 4a$ superstructure together with atoms and a 1D superstructure, inherent in the Bi-O plane, perpendicular to the b axis. The image was measured at a sample bias (V_s) of 30 mV and initial tunneling current (I_t) of 0.3 nA. (b) Profiles along the line at the same position in STM images at various bias voltages (yellow line in the top panel). The line was purposely taken to be perpendicular to axis b , that is, 45 degrees from the orientation of the $4a \times 4a$ superstructure so that the 1D superstructure of the Bi-O plane could not obscure the profile of the $4a \times 4a$ superstructure.

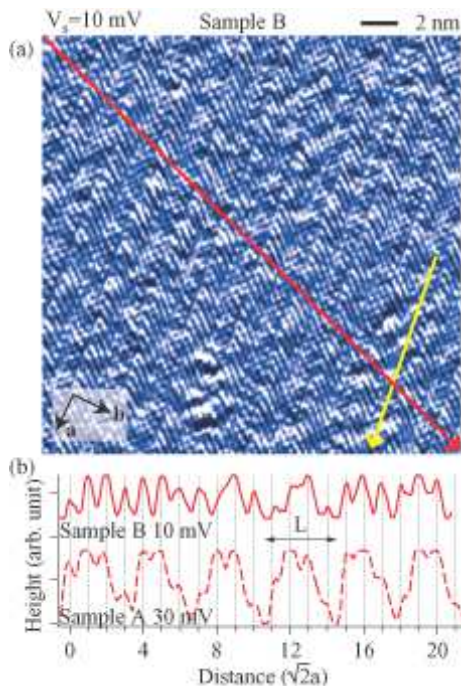


Fig. 2. (a) STM image of sample B at $T \sim 9$ K, measured at $V_s = 10$ mV, $I_t = 0.3$ nA. (b) Line profile of the STM image at $V_s = 10$ mV along the yellow line in the top panel. For comparison, the line profile of sample A at $V_s = 30$ mV (Fig. 1(b)) is also shown (broken line).

tioned below. Low-bias STM imaging is crucial to investigating the electronic structure of the Cu-O plane within the pairing gap. Such imaging is especially favorable for the study of the Cu-O plane of Bi2212. This is because, when bias voltage V_s lies within the semiconducting gap E_g (~ 200 meV) of the Bi-O plane ($V_s < E_g/e$), electron tunneling occurs predominantly not between the STM tip and the Bi-O plane but between the STM tip and the Cu-O plane.¹³ Thus low bias STM images provide information about the Cu-O plane selectively. In Fig. 1(a), we can identify a Cu-O bond-oriented, 2D superstructure with a patched structure throughout the whole STM image, which was observed for both positive and negative biases. Fig. 1(b) shows line profiles of STM images under various V_s 's, taken along the yellow line shown in Fig. 1(a). (Note that the yellow line runs parallel to the 1D superstructure, which is inherent in the Bi-O plane, to avoid crossing it.) In Fig. 1(b), we can identify a 2D superstructure with a periodicity of $4a$, namely a $4a \times 4a$ superstructure, at $V_s = 30$ and 100 mV in addition to the primitive lattice and its independence from the bias voltage. We also notice that the $4a \times 4a$ superstructure is more intense at lower bias voltage, and becomes very weak at a high $V_s = 800$ mV where only a primitive lattice is observed. The low-bias STM image for sample B is shown in Fig. 2(a), and we can also identify the 2D superstructure, not throughout the cleaved surface, but over local regions on a nanometer scale. In Fig. 2(b), the line profile of the STM image with $V_s = 10$ mV is shown for the region where the 2D superstructure appears most clearly. We can clearly see the superstructure with a periodicity of $4a$, but its amplitude is evidently smaller than that observed for sample A.

In Fig. 3, a 2D Fourier map $F(q_x, q_y)$ of the real-space STM image taken at $V_s = 30$ mV is shown for sample A. Besides Fourier peaks corresponding to the underlying primitive lattice (Bragg peaks) and the 1D superstructure of the Bi-O plane, two different Fourier peaks appear along both q_x and q_y axes: $\mathbf{q} = (1/4, 0)2\pi/a$ and $(3/4, 0)2\pi/a$, $(0, 1/4)2\pi/a$ and $(0, 3/4)2\pi/a$. The peaks along the q_x axis are stronger than those along the q_y axis. The Fourier peak at $q = 3/4 \times (2\pi/a)$ indicates that the $4a \times 4a$ superstructure has an internal structure with a period of $4a/3$. For quantitative analysis of the Fourier maps, line cuts of the 2D Fourier map along the $(\pi/a, 0)$ direction are shown as a function of V_s (Fig. 3(a)). The Fourier peaks at $q_x = 1/4 \times (2\pi/a)$ and $3/4 \times (2\pi/a)$ are most intense at the lowest bias, 20 mV, and decrease rapidly with the increase of V_s . Finally they tend to fade out above $V_s \sim 100$ mV. It should be noted here that those Fourier peaks show no change in position and no broadening even if V_s increases, indicating that the $4a \times 4a$ superstructure observed in the present STM experiments is nondispersive. The correlation length determined from the full width at half-maximum of the Fourier peak is rather short, about 6 nm. The line cuts of 2D Fourier map are also shown for sample B along the $(\pi/a, 0)$ direction (Fig. 3(b)). We can identify the $1/4 \times (2\pi/a)$ peak up to 50 mV, while the $3/4 \times (2\pi/a)$ peak is very weak. The intensity of the $1/4 \times (2\pi/a)$ peak normalized with the Bragg peak is much weaker than that for sample

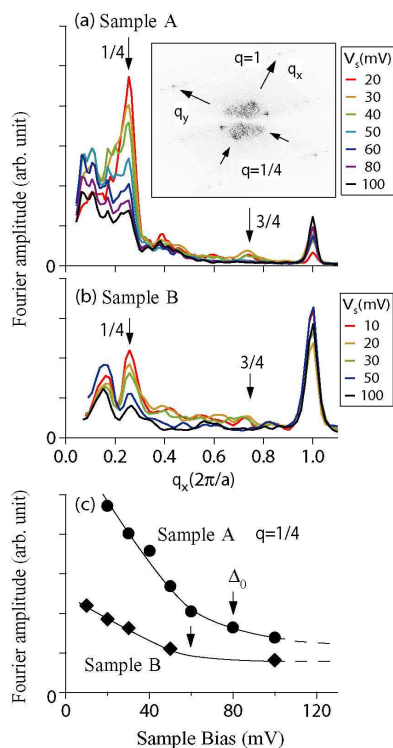


Fig. 3. (a) Line cuts of 2D Fourier maps of the STM image for sample A along $(0, 0)$ - $(0, \pi)$ at various bias voltages. Inset is a 2D Fourier map of the real-space STM image (Fig. 1(a)). (b) Line cuts of the 2D Fourier map of the STM image for sample B (Fig. 2(a)). (c) Energy dependence of the Fourier amplitude at $q = 1/4$. The arrows show the average sizes of the pairing gaps measured on the sample A and B.

A, consistent with the results of the line profiles of real-space STM images. The $1/4 \times (2\pi/a)$ peak decreases with increased bias voltage and tends to fade out at bias voltages above ~ 50 mV. Peak-like structures are observed at $q < 0.2$ in A and B samples, but they show almost no energy dependence in peak intensity, meaning that these structures are irrelevant to the superstructure that we focused on (Fig. 3(a) and (b)).

Shown in Fig. 5 is an STS spectrum, averaged over the distance of ~ 40 nm on the cleaved surface of sample A, which exhibits an intense, nondispersive $4a \times 4a$ superstructure throughout the whole STM image. For comparison, a typical ZTPG spectrum reported for lightly doped Na-CCOC is also shown in Fig. 5.²⁾ The STS spectrum of sample A has a structure very similar to the ZTPG; that is, an asymmetric V-shaped gap without coherence peaks. Width Δ_0 of the present ZTPG is ~ 80 meV on the positive bias side. In Fig. 6, the spatial dependence of STS spectra is shown for the cleaved surface of sample B whose STM image exhibits the $4a \times 4a$ superstructure locally. It should be stressed that the STS spectra of sample B are very homogeneous and show a gap structure of the d-wave type. The gap width, Δ_0 , is ~ 60 meV, though it tends to be slightly enhanced over the regions exhibiting the $4a \times 4a$ superstructure clearly. The specific,

homogeneous d-wave gap means that the doping level is rather homogeneous in sample B and the hole pairs are uniformly formed all over the cleaved surface. However the electronic $4a \times 4a$ superstructure appears only locally, as mentioned above. The dynamical $4a \times 4a$ charge order probably evolves throughout the cleaved surface of sample B, and some kind of disorder will pin down the dynamical charge order locally. It is worthwhile to point out here that in both samples A and B, the value of Δ_0 roughly corresponds to the STM bias voltage below which the $4a \times 4a$ superstructure can clearly be observed in STM imaging. This fact implies the possibility that in-gap states, namely the hole pairs, will contribute to the formation of the $4a \times 4a$ superstructure. In high- T_c cuprates, the gap size increases with the decrease in the doping level.^{14,15)} Thus, the larger gap size measured on the cleaved surface for sample A than for sample B means that the doping level of the cleaved surface of sample A is lower than that of sample B, though both samples are cut from the same single crystal. The $4a \times 4a$ superstructure is very intense in sample A and appears throughout the cleaved surface, whereas it is relatively weak in sample B and appears locally over the cleaved surface, as mentioned above. Furthermore, the low-bias STM image previously reported for nearly optimally doped Bi2212 with $\Delta_0 \sim 35$ meV exhibited no $4a \times 4a$ superstructure.¹³⁾ These results indicate that a low hole doping level favors the formation of the $4a \times 4a$ superstructure. It should be noted here that the cleaved surface of sample A has more missing atom rows within the cleaved Bi-O plane than that of sample B, which can be clearly seen in the high-bias STM images, predominantly reflecting the electronic structure of the Bi-O plane. (The high-bias STM images of the present samples will be published elsewhere.) If the missing atom rows are introduced within the Bi-O plane during the cleaving process, excess oxygen atoms will also be removed around the missing atom rows at the same time, which leads to the reduction of the average hole doping level of the Cu-O plane. Thus the high density of the random missing atom rows in the cleaved surface of sample A may be a possible reason why the average hole doping level is lower in the cleaved surface of sample A than for sample B, though both samples were cut from the same single crystal. The low density of the random missing atom rows in the cleaved surface of sample B can also explain its homogeneous electronic structure, namely the homogeneous pairing gap.

In the present experiments of low-bias STM imaging, namely Cu-O plane selective imaging, on underdoped Bi2212,¹³⁾ we confirmed that an intense, nondispersive $4a \times 4a$ superstructure was formed within the Cu-O plane. The $4a \times 4a$ superstructure has a substructure with a periodicity of $4a/3$ and is clearly observed within the pairing energy gap. Such features of the present $4a \times 4a$ superstructure are in good agreement with those of the $4a \times 4a$ electronic charge order reported for lightly doped Na-CCOC.²⁾ The intense, nondispersive $4a \times 4a$ electronic charge order is different in origin from the dispersive 2D modulation caused by quasiparticle scattering interference.⁵⁾ The present nondispersive electronic charge order is consistent with the findings of Howald

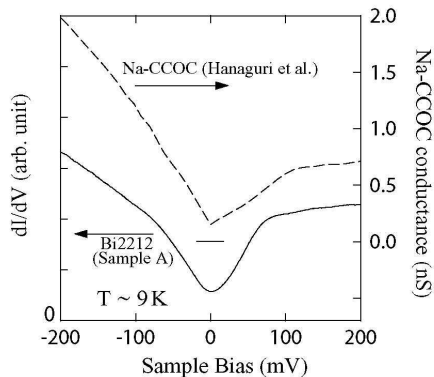


Fig. 4. STS spectrum averaged over the distance of 40 nm on the cleaved surface of sample A at $T \sim 9$ K. A typical ZTPG spectrum reported for Na-CCOC ($x=0.12$) is also shown for comparison (broken line).²⁾

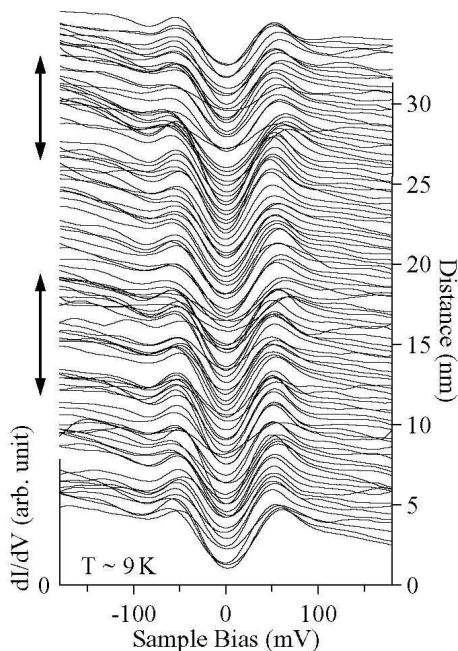


Fig. 5. Spatial dependence of STS spectra for sample B, taken at $T \sim 9$ K along the red line in Fig. 2(a). Two-headed arrows beside the spectra indicate the regions where the $4a \times 4a$ superstructure is clearly observed.

et al. in the LDOS maps for the SC state of Bi2212.^{7,8)} They claim that the nondispersive superstructure results from the formation of a static stripe order. The present results can be explained in terms of a static stripe order except for the experimental finding for sample B that the pairing gap is influenced only slightly even over

the region where the dynamical $4a \times 4a$ charge order is locally pinned down. Since the formation of the static stripe order causes the superconductivity to seriously deteriorate, as demonstrated for $\text{La}_{2-x}\text{Ba}_x\text{CuO}_4$ and $\text{La}_{1.6-x}\text{Nd}_{0.4}\text{Sr}_x\text{CuO}_4$ systems where simple 1D strips develop, the pairing gap would be seriously influenced over the region where the $4a \times 4a$ electronic charge order is pinned down. The present $4a \times 4a$ electronic charge order, clearly appearing within the pairing gap, is not inconsistent with models for the electronic charge order due to pair density waves, electronic supersolids, or paired-hole Wigner crystallization.^{16–22)}

This work was supported in part by Grants-in-Aid for Scientific Research and the 21st century COE program “Topological Science and Technology” from the Ministry of Education, Culture, Sports, Science and Technology of Japan.

- 1) M. Vershinin, S. Misra, S. Ono, Y. Abe, Y. Ando and A. Yatsudani: Science **33** (2004) 1995.
- 2) T. Hanaguri, C. Lupien, Y. Kohsaka, D-H. Lee, M. Azuma, M. Takano, H. Takagi and J. C. Davis: Nature **430** (2004) 1001.
- 3) K. McElroy, R. D-H. Lee, J. E. Hoffmann, K. M. Lang, J. Lee, E. W. Hudson, H. Eisaki, S. Uchida and J. C. Davis: cond-matt/0406491.
- 4) J. E. Hoffman, E. W. Hudson, K. M. Lang, V. Madhavan, H. Eisaki, S. Uchida, J. C. Davis: Science **295** (2002) 466.
- 5) J. E. Hoffmann, K. McElroy, D-H. Lee, K. M. Lang, H. Eisaki, S. Uchida and J. C. Davis: Science **297** (2002) 1148.
- 6) K. McElroy, R. W. Simmonds, J. E. Hoffmann, D-H. Lee, K. J. Orenstein, H. Eisaki, S. Uchida and J. C. Davis: Nature **422** (2003) 592.
- 7) C. Howald, H. Eisaki, N. Kaneko, M. Greven and A. Kapitulnik: Phys. Rev. B **67** (2003) 014533.
- 8) A. Fang, C. Howald, H. Eisaki, N. Kaneko, M. Greven and A. Kapitulnik: Phys. Rev. B **70** (2004) 214514.
- 9) S. A. Kivelson, E. Fradkin, and V. J. Emery: Nature **393** (1998) 550.
- 10) M. Bosch, W. van Saarloos, and J. Zaanen: Phys. Rev. B **63** (2001) 092501.
- 11) M. Oda, H. Matsuki, and M. Ido: Solid State Commun. **74** (1990) 1321.
- 12) T. Nakano, M. Oda, C. Manabe, N. Momono, Y. Miura, M. Ido: Phys. Rev. B **49** (1994) 16000.
- 13) M. Oda, C. Manabe and M. Ido: Phys. Rev. B **53** (1996) 2253.
- 14) M. Oda, K. Hoya, R. Kubota, C. Manabe, N. Momono, T. Nakano, M. Ido: Physica C **281** (1997) 135.
- 15) N. Miyakawa, P. Guptasarma, J. F. Zasadzinski, D. G. Hinks, K. E. Gray: Phys. Rev. Lett. **80** (1998) 157.
- 16) H. C. Fu, J. C. Davis and D-H Lee: cond-matt/0403001.
- 17) M. Vojta: Phys. Rev. B **66** (2002) 104505.
- 18) H-D Chen, O. Vafek, A Yazdani and S-H Zhang: Phys. Rev. Lett. **93** (2004) 187002.
- 19) S. Sachedev and E. Demler: Phys. Rev. B **69** (2004) 144504.
- 20) Z. Tesanovic: Phys. Rev. Lett. **93** (2004) 217004.
- 21) M. Franz: cond-mat/0409431.
- 22) P. W. Anderson: con-matt/0406038.